Complex & Intelligent Systems (2023) 9:6831–6844
https://doi.org/10.1007/s40747-023-01107-2

ORIGINAL ARTICLE

A novel fractional-order flocking algorithm for large-scale UAV swarms

Haotian Chen[1] · Ming He[1] · Jintao Liu[1] · Peng Xu[1] · Xianghui Cao[2] · Wei Han[1] · Guodong Yuan[1]

Received: 4 January 2023 / Accepted: 8 May 2023 / Published online: 5 June 2023

Abstract
The rate of convergence is a vital factor in determining the outcome of the mission execution of unmanned aerial vehicle (UAV) swarms. However, the difficulty of developing a rapid convergence strategy increases dramatically with the growth of swarm scale. In the present work, a novel fractional-order flocking algorithm (FOFA) is proposed for large-scale UAV swarms. First, based on the interaction rules of repulsion, attraction and alignment among swarm individuals, fractional calculus is introduced to replace traditional integer-order velocity updating, which enables UAVs to utilize historical information during flight. Subsequently, the convergence of the algorithm is theoretically analyzed. Some sufficient convergence conditions for the FOFA are presented by exploiting graph theory. Finally, the simulation results validate that our proposed FOFA performs much better than traditional flocking algorithms in terms of convergence rate. Meanwhile, the relationships between the fractional order of the FOFA and the convergence time of the UAV swarm are discussed. We find that under certain conditions, the fractional order is strongly correlated with the convergence rate of the UAV swarm; that is, a small fractional order (more consideration of historical information) leads to better performance. Moreover, the fractional order can be used as an important parameter to control the convergence rate of a large-scale UAV swarm.

Keywords Fractional calculus · Large-scale UAV swarms · Flocking · Convergence rate

Introduction

Unmanned aerial vehicles (UAVs) have been widely used in industry, the military and agriculture due to their low cost and small size. To further develop the superiority of UAVs and to improve the efficiency of missions, the concept of UAV swarms was developed. In comparison with a single UAV, UAV swarms are more flexible and robust and have much broader application potential in unmanned combat, surveillance, rescue and many other fields. Therefore, large-scale UAV swarms are mainly considered in this paper.

For large-scale UAV swarms, rapid convergence is the premise for the smooth execution of various tasks. Specifically, UAV swarms are disordered before performing missions. Once a mission is assigned, individuals need to assemble and to synchronize their status so that UAV swarms can reach the target areas as quickly as possible. Thus, the faster the convergence rate is, the higher the efficiency of UAV swarms. As a result, it is of great significance to develop an effective and efficient control strategy to reduce the convergence time for large-scale UAV swarms. However, due to the complexity of interactions between UAVs and changing environments, designing this kind of strategy remains challenging.

By studying biological groups with intelligence characteristics, such as cells, insects, fish schools and birds flocks [1–4], researchers proposed the concept of flocking

✉ Ming He
ming_he_2020@126.com

Haotian Chen
cht13505151880@163.com

Jintao Liu
Jintao_liu_2020@126.com

Peng Xu
xupeng@aeu.edu.cn

Xianghui Cao
xhcao@seu.edu.cn

Wei Han
mxyacc@nuaa.edu.cn

Guodong Yuan
305551544@qq.com

1 Command and Control Engineering College, Army Engineering University of PLA, Houbiaoying 210007, Nanjing, China

2 School of Automation, Southeast University, Sipailou 210096, Nanjing, China

control, which has the characteristics of adaptability, robustness, dispersion and self-organization; flocking control is quite compatible with the robustness and self-organization required by UAV swarms. Hence, it is meaningful to study the flocking control of UAV swarms at large scales.

Various flocking models and algorithms have been applied in large-scale UAV swarms. Yan [5] proposed a curriculum-based multiagent deep reinforcement learning (MADRL) approach to address the flocking and collision avoidance problem for a large-scale fixed-wing UAV swarm. Wang [6] presented an oracle-guided two-stage training and execution scheme for large-scale UAV swarms, which enables flocking and navigation control under a limited communication range. Jia [7] investigated the three-dimensional leaderless flocking problem for large-scale small UAV swarms and proposed a simplified distributed control algorithm on the basis of existing flocking algorithms. Liu and He [8] studied the substructures in large-scale UAV swarms based on the Olfati-Saber flocking model [9], providing a new idea for the cooperative control model of UAV swarms. In 2019, Jia and Vicsek [10] presented a hierarchical flocking model (HVEM) by introducing a layered mechanism into the traditional Vicsek model [11]. On the basis of HVEM, Liu [12, 13] proposed a hierarchical weighting Vicsek model (HWVEM) and investigated the flocking navigation as well as obstacle avoidance of UAV swarms. The existing flocking control methods for large-scale UAV swarms mostly focus on specific task scenarios, such as collision avoidance, navigation and obstacle avoidance. However, with respect to the convergence rate, which is a key factor in ensuring that UAV swarms perform tasks successfully, there are very few related studies, and the results are primarily established under the framework of integer-order dynamics. For instance, Zhao [14] proposed a modified adaptive-velocity self-organizing model to enhance the convergence of the Couzin model in a high-speed environment. Lu [15] improved the neighbor selection strategy of the Vicsek model by selecting individuals with only a large degree as neighbors, which made the directions of all particles' motions reach consensus more quickly. Zhao [16] introduced a local consistency parameter into the Vicsek model to reduce the convergence time. These methods are circumscribed for improving the convergence rate of UAV swarms. On the one hand, these methods simply change the interaction rules, potential functions and algorithm parameters of the flocking models, while the dynamics of UAVs, which are fundamental to controllers and have a greater influence on the convergence rate, are not taken into consideration. On the other hand, the individuals update their states by considering the information only for the current moment. Nevertheless, in actual collective motion, intelligent agents often use historical information in the decision process to achieve better performance [17, 18]. In addition, strict mathematical proofs were not given in terms of the convergence of swarms in those methods. All of these factors add difficulty to the control of large-scale UAV swarms.

Recently, fractional calculus (FC) has been successfully applied in science and engineering, such as the control of multiagent systems [19, 20] and the analysis of internal structures of fractal functions [21, 22]. FC is believed to be a good way to address certain physical system modeling problems [23, 24] and to improve the convergence rate of intelligent systems [25, 26]. Yousri [27] improved the convergence of the manta ray foraging optimizer by introducing FC into the motion process of manta rays. To shorten the convergence time of neural networks, Dong [28] proposed an FC-based gradient descent method, and the simulations showed that the convergence time can be reduced by nearly 10% compared to that of the integer order approach. The most significant characteristic of fractional-order systems is that the current state depends on the whole history [29], and due to this property, many phenomena that cannot be explained naturally by integer-order dynamics can be explained by the coordinated behavior of agents with fractional-order dynamics, such as the spread of virus and the motion of telomeres in the nucleus of mammalian cells [30, 31]. Therefore, to develop a control strategy with rapid convergence for large-scale UAV swarms, it is necessary to apply FC to the dynamic design of UAVs.

Inspired by the above research, a modified flocking algorithm incorporating fractional calculus in the updating process of UAV swarms, namely, the fractional-order flocking algorithm (FOFA), is proposed in this paper. This algorithm allows UAVs to utilize historical information in flight and can greatly shorten the convergence time. The main contributions of this paper are the following:

(1) A fractional-order flocking algorithm (FOFA) is proposed by replacing the usual integer-order derivative with a fractional derivative, which enables UAVs to utilize historical information during the decision process, thus overcoming the shortage of traditional ordinary differential methods that consider only the current information.
(2) The convergence of the FOFA is theoretically analyzed. By exploiting graph theory, a sufficient convergence condition is given.
(3) To validate the effectiveness of the proposed algorithm, simulations are conducted with various scales and types of UAV swarms. The results indicate that in comparison with traditional integer-order flocking algorithms, the FOFA can significantly improve the convergence rate of large-scale UAV swarms.
(4) We find that the convergence rate is strongly correlated with the fractional order of the FOFA under the condition that the scale of the UAV swarm is large, that is, a small fractional order (more consideration of historical information) leads to better performance, and the fractional

order can be used as an important parameter to control the convergence rate of a large-scale UAV swarm.

The rest of this paper is organized as follows. In Preliminaries, the definitions of fractional calculus and basic concepts of graph theory are given. In Fractional-order flocking algorithm, we first introduce the FOFA, and then, the stability of FOFA is theoretically analyzed. In Simulations and results, we provide simulations and corresponding result analysis to verify our work. Finally, the paper is concluded.

Preliminaries

In this section, the definitions for fractional calculus are given, and then some sufficient lemmas and elementary concepts about graph theory are introduced.

Fractional calculus

The Grünwald–Letnikov (G-L) fractional derivative was introduced in a general form by Liouville, considered by some of the father of fractional calculus. This formula plays an important role in solving numerical problems and generalizes ordinary differentiation. The definition of the G-L fractional derivative is as follows [32]:

Let $\alpha \in (0, 1]$, $h > 0$, then

$$D^{\alpha}(x(t)) = \lim_{h\to 0}\left(\frac{1}{h^{\alpha}}\sum_{k=0}^{+\infty}\frac{(-1)^k\Gamma(\alpha+1)x(t-kh)}{\Gamma(k+1)\Gamma(\alpha-k+1)}\right) \quad (1)$$

is called the G-L fractional derivative of $x(t)$ of order α.

Now, we consider a discrete-time commensurate fractional order system with the following state space equations:

$$D^{\alpha}(x(k+1)) = Fx(k) + Gu(k), \quad (2)$$

where $x(k) \in \mathbb{R}^n$ is the state vector and $u(k) \in \mathbb{R}^m$ is the input signal. $F \in \mathbb{R}^{n\times n}$ and $G \in \mathbb{R}^{n\times m}$ are the space matrices, and $D^{\alpha}(x(k))$ is given by

$$D^{\alpha}(x(k)) = \frac{1}{T^{\alpha}}\sum_{t=0}^{m}\frac{(-1)^k\Gamma(\alpha+1)x(k-tT)}{\Gamma(t+1)\Gamma(\alpha-t+1)}, \quad (3)$$

where T is the sampling period, m is the truncation order and $\Gamma(\cdot)$ is the Gamma function.

An important characteristic revealed by Eq. (3) is that there are an infinite number of terms in the fractional-order derivative, while the integer-order derivative implies only a finite series. Consequently, integer-order derivatives are "local" operators, whereas fractional-order derivatives implicitly have a "memory" of all past events.

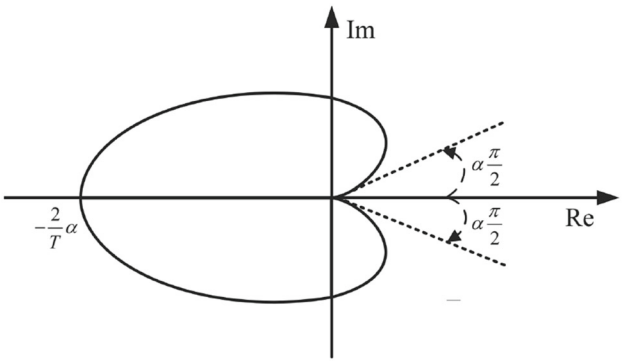

Fig. 1 The stability region for discrete-time fractional-order system (2) [35]

Lemma 1 [33, 34] *The fractional-order system* (2) *is said to be asymptotically stable if and only if*

$$\varphi_i^F \in \left[\frac{\pi}{2}, 2\pi - \frac{\pi}{2}\right] \wedge |\lambda_i^F| < |\omega_i|, \quad (4)$$

where λ_i^F *represents the* i*th eigenvalue of* F, φ_i^F *denotes the argument of* λ_i^F *and* $|\omega_i|$ *is given as*

$$|\omega_i| = \left(\frac{2}{T}\left|\sin\frac{\varphi_i^F - \frac{\alpha\pi}{2}}{2-\alpha}\right|\right)^{\alpha}. \quad (5)$$

The geometric interpretation is shown in Fig. 1. *It is obvious that system* (2) *is stable if all* λ_i^F *lie inside the determined region in Fig.* 1.

Graph theory

Graph theory is utilized to describe the interaction among agents in UAV swarms. Some fundamental concepts about graph theory and the Laplacian matrix are given in the following.

A graph G with N nodes is denoted by $G = (S, E)$, where $S = \{1, 2, \ldots, N\}$ is a nonempty finite set of nodes and $E \subseteq S \times S$ is the set of edges, in which an edge is represented by $e_{ij} = \{i, j\}$. The set of neighbors of node i is denoted by $\mathcal{N}_i = \{j \in S : (j, i) \in E\}$. $A = [a_{ij}]_{N\times N}$ is the adjacency matrix of graph G, where a_{ij} is the weight of edge $\{j, i\}$. If $\{j, i\} \in E$, then $a_{ij} = 1$; otherwise, $a_{ij} = 0$. The Laplacian matrix of graph G is defined as $L = [l_{ij}]_{N\times N}$ with $l_{ii} = \sum_{j\neq i} a_{ij}$ and $l_{ij} = -a_{ij}$ for $i \neq j$.

Lemma 2 *The Laplacian matrix of undirected connected graphs has one zero eigenvalue with eigenvector 1, and all of its nonzero eigenvalues are real and positive* [36].

Fractional-order flocking algorithm

In this section, a flocking algorithm based on the G-L fractional derivative is proposed to control the UAV swarm. First, the dynamics based on the Vicsek model are given, and then G-L fractional calculus is introduced into the decision-making process such that historical information is considered when individuals update their velocity. The algorithm is as follows.

Dynamics of UAVs

We assume that there are N UAVs working in two-dimensional Euclidean spaces with a common initial absolute value of velocity. The dynamics of UAVs are determined by their distance, which are given as follows.

Repulsion force

The repulsion force is used to prevent collisions between UAVs, and it exists only when the distance between any two UAVs is smaller than the repulsive radius r_{rep}. We denote $x_i(t) \in \mathbb{R}^2$ as the position of UAVi at time t. The definition of repulsion force is

$$f_i^{\text{rep}}(t+1) = c_{rep} \sum_{j \in \mathcal{N}_i(t)} a_{ij}(t) \left(\frac{r_{rep} - \|x_{ij}(t)\|}{r_{rep}} \cdot \frac{x_{ij}(t)}{\|x_{ij}(t)\|} \right), \tag{6}$$

where $x_{ij}(t) = x_j(t) - x_i(t)$, r_{rep} and c_{rep} are the repulsion radius and the coefficient of repulsion force, respectively. $\mathcal{N}_i(t) = \{j \| \|x_i(t) - x_j(t)\| \le r\}$. Here, r denotes the communication radius of UAVs.

Attraction force

The attraction force is used to keep the swarm tight, and it is considered only when the distance of two UAVs is between communication radius r and repulsion radius r_{rep}.

$$f_i^{\text{att}}(t+1) = c_{att} \sum_{j \in \mathcal{N}_i(t)} a_{ij}(t) \left(\frac{r_{rep} - \|x_{ij}(t)\|}{r - r_{rep}} \cdot \frac{x_{ij}(t)}{\|x_{ij}(t)\|} \right), \tag{7}$$

where c_{att} is the coefficient of attraction force.

Alignment force

The alignment force is used to keep all the UAVs moving in the same direction, which is based on the Vicsek model [11], and the definition is [37]

$$f_i^{\text{align}}(t+1) = \frac{c_{align}}{1+d_i} \left(v_i(t) + \sum_{j \in \mathcal{N}_i(t)} a_{ij}(t) v_j(t) \right), \tag{8}$$

where c_{align} is the coefficient of the alignment force and $v_i(t) \in \mathbb{R}^2$ is the velocity of UAVi at time t.

Above all, the interaction forces between UAVi and other swarm members at time t are

$$u_i(t) = f_i^{\text{att}}(t) + f_i^{\text{rep}}(t) + f_i^{\text{align}}(t). \tag{9}$$

Movement of UAVs

Without loss of generality, we suppose that the time interval Δt between two updates of the velocities and positions is 1. The position of UAVi at time $t+1$ is

$$x_i(t+1) = x_i(t) + v_i(t)\Delta t. \tag{10}$$

In the general flocking algorithms (for details, see [38–40]), the velocity updating process is based on integer-order dynamics:

$$v_i(t+1) = v_i(t) + u_i(t)\Delta t. \tag{11}$$

Knowing that $\Delta t = 1$, Eq. (11) can be written as $v_i(t+1) - v_i(t) = u_i(t)$, that is,

$$D^1(v_i(t+1)) = u_i(t). \tag{12}$$

To apply fractional calculus to improve the convergence rate of the UAV swarm, the integer-order derivative is replaced by the fractional-order derivative; thus, we have the following relation:

$$D^\alpha(v_i(t+1)) = u_i(t), \tag{13}$$

where α is the fractional order. By the definition of the G-L fractional derivative in Fractional calculus, the expression of Eq. (13) with $T = 1$ can be written as

$$D^\alpha(v_i(t+1)) = \sum_{k=0}^{m} \frac{(-1)^k \Gamma(\alpha+1) v_i(t+1-k)}{\Gamma(k+1)\Gamma(\alpha-k+1)} = u_i(t). \tag{14}$$

Using the first $m = 4$ terms from the historical data with fractional order α, the fractional-order velocity updating of UAVi at time t is

$$\begin{aligned} v_i(t+1) = {} & \alpha v_i(t) + \frac{1}{2}\alpha(1-\alpha) v_i(t-1) \\ & + \frac{1}{6}\alpha(1-\alpha)(2-\alpha) v_i(t-2) \end{aligned}$$

$$+\frac{1}{24}\alpha(1-\alpha)(2-\alpha)(3-\alpha)v_i(t-3)+u_i(t). \tag{15}$$

The general flocking algorithm with integer-order dynamics is a particular case of FOFA with fractional order $\alpha = 1$; that is, historical information is not considered. As α decreases, the proportion of the current state information declines, while that with historical information increases.

Convergence Analysis of FOFA

In this part, the convergence of our proposed FOFA is analyzed, and the sufficient conditions to ensure the convergence of the FOFA are given. The method used in this section follows [35, 41].

By Eqs. (6)–(10) and (13), the dynamics of UAVs can be described as

$$\begin{cases} x_i(t+1) = v_i(t), \\ D^{\alpha}(v_i(t+1)) = u_i(t), \end{cases} \quad i = 1, 2, \ldots, N, \tag{16}$$

where

$$u_i(t) = \sum_{j\in\mathcal{N}_i} k_{ij}(t)a_{ij}(t)x_{ij}(t) + \frac{m}{1+d_i(t)}\left(v_i(t) + \sum_{j\in\mathcal{N}_i} a_{ij}(t)v_j(t)\right). \tag{17}$$

$d_i(t)$ is the number of neighbors of UAVi at time t, $m = c_{align}$ is a constant, $k_{ij}(t)$ is the feedback control gain, and the definition of $k_{ij}(t)$ is

$$\begin{cases} k_{ij}(t) = \frac{c_{att}(r_{rep}-\|x_{ij}(t)\|)}{(r-r_{rep})\|x_{ij}(t)\|}, & r_{rep} < \|x_{ij}(t)\| < r, \\ k_{ij}(t) = \frac{c_{rep}(r_{rep}-\|x_{ij}(t)\|)}{r_{rep}\|x_{ij}(t)\|}, & 0 \le \|x_{ij}(t)\| < r_{rep} \end{cases}. \tag{18}$$

Let $x(t) = [x_1(t), x_2(t), \ldots, x_N(t)]^T$, $v(t) = [v_1(t), v_2(t), \ldots, v_N(t)]^T$. We suppose that $K = [k_{ij}(t)]_{N\times N}$ and $B = \mathrm{diag}[b_1(t), b_2(t), \ldots, b_N(t)]$ with $b_i(t) = \sum_{j\neq i} k_{ij}(t)$, then Eq. (16) can be written as

$$\begin{bmatrix} x(t+1) \\ D^{\alpha}(v(t+1)) \end{bmatrix} = C\begin{bmatrix} x(t) \\ v(t) \end{bmatrix}, \quad C = \begin{bmatrix} 0 & I_N \\ -\bar{L} & mP \end{bmatrix} \tag{19}$$

where I_N is an $N \times N$ identity matrix and $\bar{L} = B - K$. $P = (I_N + D)^{-1}(A + I_N)$, where $D = \mathrm{diag}[d_1(t), d_2(t), \ldots, d_N(t)]$. It is obvious that the convergence of the FOFA described by Eq. (16) is realized if system (19) is asymptotically stable.

Corollary 1 *All the eigenvalues of P are positive real numbers.*

Proof According to the definition of P, we can obtain $P = \mathrm{diag}[\frac{1}{1+d_1(t)}, \frac{1}{1+d_2(t)}, \ldots, \frac{1}{1+d_N(t)}]$, where $d_i(t)$ is the number of neighbors of UAVi; therefore, $\mu_{2i} = \frac{1}{1+d_i(t)} > 0$. This completes the proof. □

Corollary 2 *Let μ_{1i}, $i = 1, 2, \ldots, N$ be the eigenvalues of $\bar{L}$. If $c_{att} < 0$, it holds that*

$$0 = \mu_{11} \le \mu_{12} \le \cdots \le \mu_{1N}. \tag{20}$$

Proof Since $\bar{L} = B - K$, according to the definition of B and K, we can obtain that the elements of $\bar{L}$ are $\bar{l}_{ij} = -k_{ij}(t)a_{ij}(t)$ for $i \neq j$ and $\bar{l}_{ii} = \sum_{j\neq i} k_{ij}(t)a_{ij}(t)$. Then,

$$x(t)^T\bar{L}x(t) = \sum_{a_{ij(t)}=1} k_{ij}(t)(x_i(t) - x_j(t))^2 \ge 0. \tag{21}$$

Hence, $\bar{L}$ is a semipositive definite matrix, which means that Corollary 2 holds. □

Now, we consider Eq. (19). We suppose that the eigenvalue of C is λ; then, we have

$$\begin{aligned} \det(\lambda I_{2N} - C) &= \det\begin{bmatrix} \lambda I_N & -I_N \\ \bar{L} & \lambda I_N - mP \end{bmatrix} \\ &= \det(\lambda I_N)\det(\lambda^2 I_N - m\lambda P + \bar{L}) \\ &= \prod_{i=1}^{N}(\lambda^2 - m\lambda\mu_{2i} + \mu_{1i}), \end{aligned} \tag{22}$$

where μ_{1i} and μ_{2i} are the ith eigenvalues of $\bar{L}$ and P, respectively. Solving Eq. (22), we obtain

$$\begin{cases} \lambda_{i1} = \frac{m\mu_{2i}+\sqrt{m^2\mu_{2i}^2-4\mu_{1i}}}{2}, \\ \lambda_{i2} = \frac{m\mu_{2i}-\sqrt{m^2\mu_{2i}^2-4\mu_{1i}}}{2}, \end{cases} \quad i = 1, 2, \ldots, N. \tag{23}$$

It can be seen that λ_{i1} and λ_{i2} can be complex numbers, so condition (4) may give complicated relations in terms of m. To produce explicit inequalities in terms of m, the parameters are chosen so that all the eigenvalues are real numbers. This means

$$m^2\mu_{2i}^2 - 4\mu_{1i} \ge 0 \quad i = 1, 2, \ldots, N, \tag{24}$$

relation (24) leads to

$$m \ge \frac{2\sqrt{\mu_{1\max}}}{\mu_{2\min}} \quad or \quad m < -\frac{2\sqrt{\mu_{1\min}}}{\mu_{2\max}}. \tag{25}$$

Considering that $\mu_{1\min} = 0$, then relation (25) can be written as

$$m \geq \frac{2\sqrt{\mu_{1\max}}}{\mu_{2\min}} \quad or \quad m < 0. \tag{26}$$

According to Corollary 1 and Corollary 2, all $\mu_{1i} \geq 0$ and $\mu_{2i} > 0$. If $m \geq 0$, both λ_{i1} and λ_{i2} are nonnegative, that is,

$$\varphi_i = \arg(\lambda_{i1}) = \arg(\lambda_{i2}) = 0, \quad i = 1, 2, \ldots, N. \tag{27}$$

It is obvious that all λ_i are on the right side of the Re-axis of Fig. 1, which cannot satisfy the argument condition in Eq. (4). However, if $m < 0$ is considered, both λ_{i1} and λ_{i2} are negative, which means

$$\varphi_i = \arg(\lambda_{i1}) = \arg(\lambda_{i2}) = \pi, \quad i = 1, 2, \ldots, N. \tag{28}$$

We consider that $\pi \in [\frac{\alpha\pi}{2}, 2\pi - \frac{\alpha\pi}{2}]$; thus, the argument condition in Eq. (4) is satisfied. Therefore,

$$m < -\frac{2\sqrt{\mu_{1\min}}}{\mu_{2\max}}. \tag{29}$$

Now, we consider the absolute value condition in Eq. (4). By Eq. (5) and Eq. (28), we have

$$|\omega_i| = \left(\frac{2}{T}\left|\sin\frac{\pi - \frac{\alpha\pi}{2}}{2-\alpha}\right|\right)^{\alpha} = \frac{2^{\alpha}}{T^{\alpha}} \quad i = 1, 2, \ldots, N. \tag{30}$$

It is easy to check that $|\lambda_{i1}| < |\lambda_{i2}|$, then by Eq. (4), we obtain

$$|\lambda_{i2}| = \frac{-m\mu_{i2} + \sqrt{m_2^2\mu_{2i}^2 - 4\mu_{1i}}}{2} < \frac{2^{\alpha}}{T^{\alpha}}. \tag{31}$$

The above relation leads to

$$\sqrt{m^2\mu_{2i}^2 - 4\mu_{1i}} < \frac{2^{\alpha+1}}{T^{\alpha}} + m\mu_{2i}. \tag{32}$$

The right side of relation (32) should be positive; thus,

$$m > -\frac{2^{\alpha+1}}{T^{\alpha}\mu_{2\max}}. \tag{33}$$

According to (32),

$$m > -\left(\frac{T^{\alpha}\mu_{1\min}}{2^{\alpha}\mu_{2\max}} + \frac{2^{\alpha}}{T^{\alpha}\mu_{2\max}}\right) \tag{34}$$

We consider that $\mu_{1\min} = 0$; then, we have

$$m > -\left(\frac{T^{\alpha}\mu_{1\min}}{2^{\alpha}\mu_{2\max}} + \frac{2^{\alpha}}{T^{\alpha}\mu_{2\max}}\right) = -\frac{2^{\alpha}}{T^{\alpha}\mu_{2\max}}$$

$$> -\frac{2^{\alpha+1}}{T^{\alpha}\mu_{2\max}} \tag{35}$$

Now, we can obtain the following theorem.

Theorem 1 *The sufficient condition to achieve convergence of the FOFA given in Eqs. (16)–(18) is*

$$-\frac{2^{\alpha+1}}{T^{\alpha}\mu_{2\max}} < m < 0, \tag{36}$$

where $\mu_{2\max}$ is the maximum eigenvalue of P.

Remark 1 Condition (36) is conservative because condition (4) may also be fulfilled when the eigenvalues of C are complex numbers. That is why only the sufficient convergence condition for FOFA is obtained.

Flow chart of FOFA

Based on the above design, the flow chart of FOFA is shown in Fig. 2. After initializing the parameters of the FOFA, the interaction forces are adopted to achieve flocking, namely, the alignment force, the repulsion force and the attraction force in Eqs. (6)–(9). Then, the fractional-order dynamics are introduced into the velocity updating process of UAVs by Eq. (15), which improves the convergence rate of UAV swarms, and the order parameters are calculated, given by Eq. (37) and Eq. (38) in Order parameters.

Simulations and results

To verify the superiority of the FOFA proposed in this paper in improving the convergence rate of UAV swarms, simulation results and performance analysis based on MATLAB are given in this section. First, the parameter settings are given. Next, we give the order parameters to describe the state of UAVs during flight, and then, specific experiments and analyses are conducted for UAV swarms at various scales and types. Finally, the influence of the FOFA on the convergence rate of the UAV swarm is analyzed in detail, and the relationship between the fractional order and performance is given.

Experimental configuration and parameter settings

The UAV swarm in this paper is composed of N agents, the communication radius $r = 2$, the repulsion radius $r_{rep} = 1$, and the coefficient values of the attraction force, the repulsion force and the alignment force are $c_{att} = 0.01$, $c_{rep} = 0.2$ and $c_{align} = 0.3$, respectively. The UAVs are generated randomly in a square with length $L = 7$ and can move without any boundary limitations. All the UAVs have the same initial and maximum absolute value of velocities, which are $v_0 =$

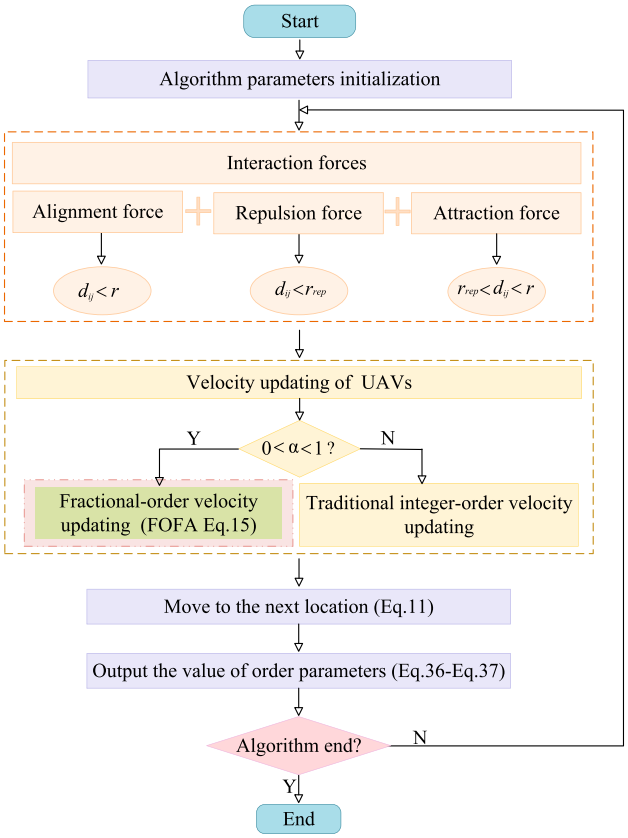

Fig. 2 Flow chart of FOFA

0.03 and $v_{max} = 0.1$. The maximum number of iterations of FOFA is 200, and the results are the average value of 100 simulations. Unless otherwise specified, all simulations follow the above settings.

Order parameters

The motion state of UAV swarms can be quantitatively expressed by two order parameters, namely:

(1) Overall velocity direction order parameter

$$\Phi_1 = \frac{1}{N}\left\| \sum_{i=1}^{N} \frac{v_i(t)}{\|v_i(t)\|} \right\|. \tag{37}$$

(2) Local velocity direction order parameter

$$\Phi_2 = \frac{1}{N}\left\| \sum_{i=1}^{N} \sum_{j\in\mathcal{N}_i(t)} \frac{1}{d_i(t)} \cdot \frac{v_i(t)v_j(t)}{\|v_i(t)\|\|v_j(t)\|} \right\|, \tag{38}$$

where $d_i(t)$ is the number of neighbors of UAVi at time t.

Φ_1 describes the degree of order of all UAV movements. As shown in Fig. 3. When $\Phi_1 = 0$, all UAVs in the swarm move in complete disorder. When $\Phi_1 = 1$, all UAVs move in the same direction, and the swarm is ultimately ordered. It has been found that the ordering is very strong when $\Phi_1 = 0.9$ in a swarm [42]. Φ_2 indicates the degree of order of local UAV movement under various conditions. Compared with Φ_1, Φ_2 can provide a stricter stability description when the swarm is divided into several coherently moving subgroups.

Performance of FOFA

The scale of the UAV swarm is an important factor to be considered in practical applications. On the one hand, if the scale is too large, the cost increases considerably; on the other hand, the expected performance may not be achieved when the scale is small. To this end, the number of UAVs in swarms is set to $N = 50$, 100, 200, 300, and 400, corresponding to different swarm levels. We define $t_c = min_{\Phi_1 \geq 0.9}$ and $t_s = min_{\Phi_2 \geq 0.99}$ as the times to achieve overall convergence and local convergence, respectively, which describe the minimum times to reach $\Phi_1 = 0.9$ and $\Phi_2 = 0.99$. A series simulations are conducted to comprehensively analyze the effectiveness of our proposed FOFA.

FOFA in a single-layer UAV swarm

For a single-layer UAV swarm, all UAVs have equal status, there are no leaders or followers, communications between each pair of UAVs are bidirectional, and all UAVs have the same contribution value. Figure 4 shows the overall and local convergence times for the FOFA-based single-layer UAV swarm under the various scales and fractional orders. When $\alpha = 1$, the FOFA is equivalent to integer-order flocking. It can be seen that:

(1) When the fractional order is constant, the convergence time of the UAV swarm increases with increasing scale, which conforms to intuition; that is, the larger the swarm scale is, the longer the convergence time.
(2) Compared with integer-order flocking, under the condition that scales are small ($N = 50$, 100), FOFA cannot significantly improve the performance of the UAV swarm, or even worse. This is because when the scale is small, the convergence rate of the cluster is fast. For example, when the cluster size is 50, convergence can be realized within 20 iterations. In this case, the commonly used integer-order dynamics can achieve rapid convergence, while the characteristics of fractional-order dynamics memory cannot be well utilized.

However, as the scale increases, the time for the FOFA-based UAV swarm to achieve overall and local convergence is greatly reduced, which indicates that under the condition that the scales of UAV swarms is large ($N \geq 200$), the FOFA has a better performance than traditional methods.

Fig. 3 The status of UAV swarm

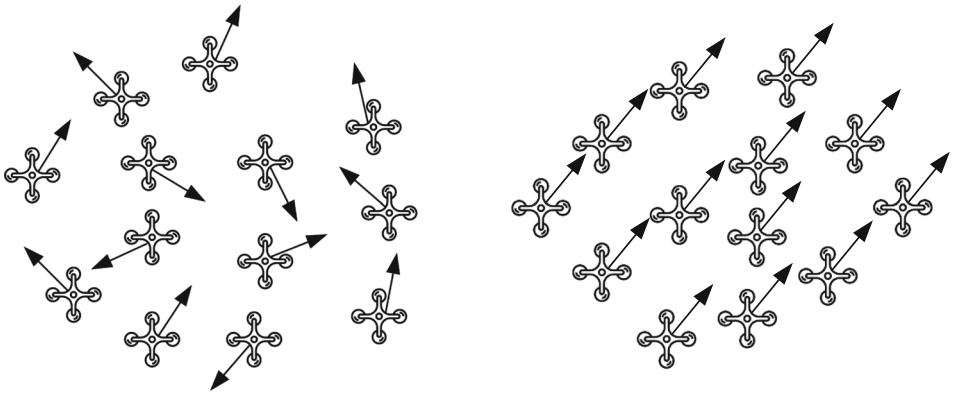

(a) Disorder **(b)** Order

Fig. 4 Convergence time of FOFA-based single-layer UAV swarm at different scales and fractional orders

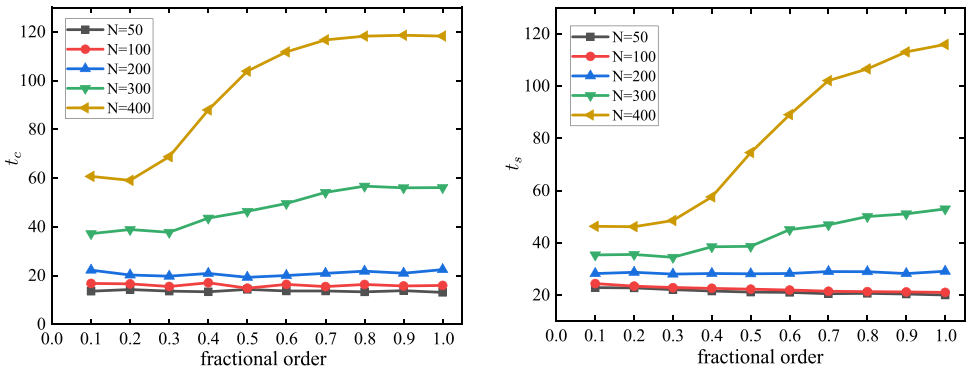

(a) Average overall convergence time **(b)** Average local convergence time

Taking $N = 300$ as an example, the four graphs in Fig. 5 show the positions and motions at different times. Figure 6a, b show the variation in Φ_1 and Φ_2 over time for an FOFA-based swarm with 300 UAVs. We can see that at the beginning of flocking, the whole swarm is disordered, which is reflected by the values of Φ_1 and Φ_2. With an increase in iterations, the degree of order of the swarm is improved through interactions between UAVs and finally reaches a convergent state. During this process, the performance of the UAV swarm based on FOFA is always better than that of integer-order flocking ($\alpha = 1$). Moreover, $\alpha = 0.1$ corresponds to the best performance, with the value of α increasing, the rates of both overall and local convergence are reduced, and when $\alpha = 1$, the performance is the worst. The specific convergence time corresponding to the various fractional orders of FOFA is shown in Table 1, where bolded font indicates optimal convergence time.

To further illustrate the advantages of the proposed FOFA, we compare it with three kinds of commonly used flocking model VEM [11], HVEM [10] and WHVEM [12]. VEM is the most basic integer-order flocking model, where there are only alignment, attraction and repulsion between particles. HVEM is a contribution-driven hierarchical system, where particles are divided into leader and follower types by their contribution weight. WHVEM consists of a hierarchical weighting mechanism and a layer regulation mechanism, and this approach improved the HVEM. The selected system is composed of 300 UAVs. To avoid randomness and to obtain general results, 100 simulations are conducted, and the maximum number of iterations of each simulation is 200. The results are shown in Fig. 7. We can see that our proposed FOFA has the most rapid convergence rate among these methods, which verifies the superiority of this algorithm. Above all, we can conclude that for a single-layer UAV swarm with a large scale, compared with the integer-order flocking algorithm, the FOFA can greatly enhance its convergence rate.

FOFA in wind environment

In order to verify the effectiveness of the FOFA in an environment with physical constraints, simulations of FOFA of UAV swarms under wind environment are carried out. Set a multi-direction sequential air flow as [40]

$$\begin{cases} v_x = c_w \sin(t + \frac{\pi t}{4}) \\ v_y = c_w \cos(t + \frac{\pi t}{4}) \end{cases}, \tag{39}$$

where c_w is a positive real number. Because there is air flow in environment, then according to Eq. (9), the interaction

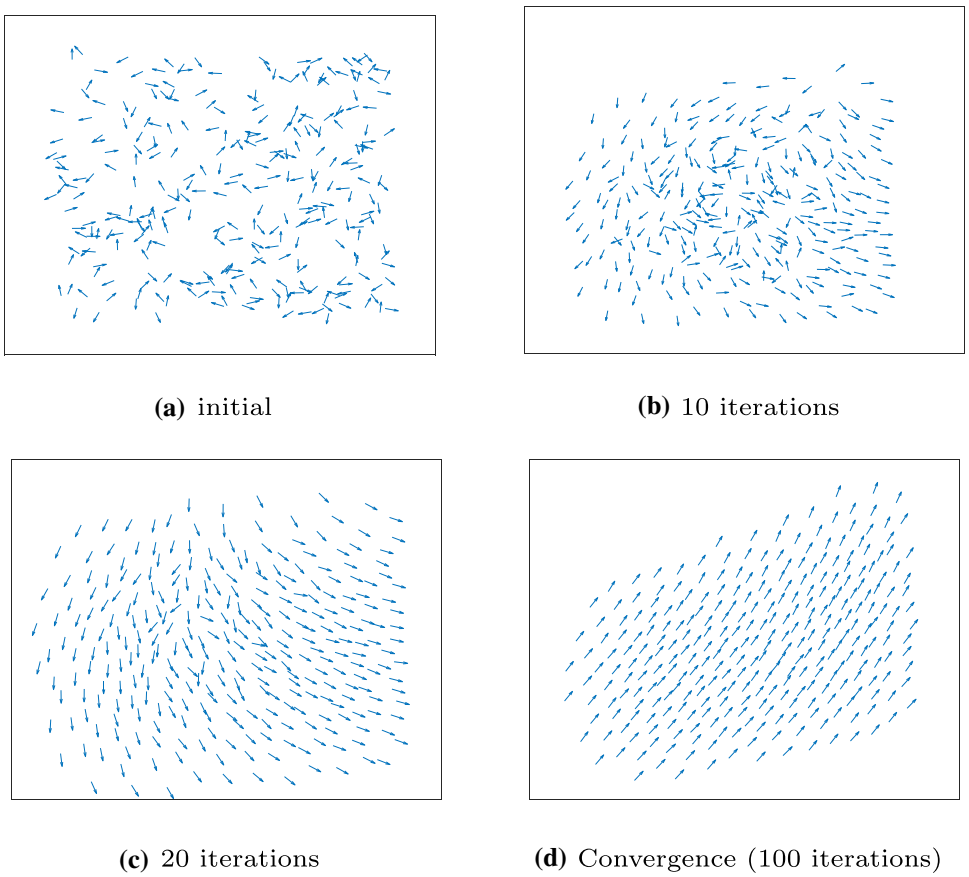

(a) initial **(b)** 10 iterations

(c) 20 iterations **(d)** Convergence (100 iterations)

Fig. 5 The positions and directions of 300 UAVs at different times

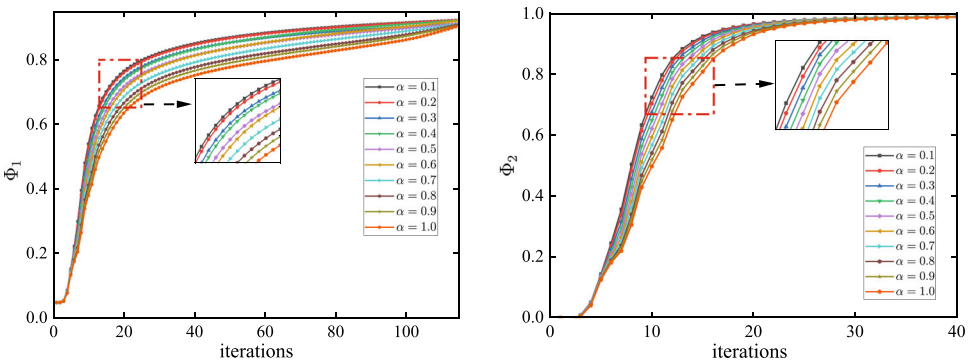

(a) Overall velocity direction order **(b)** Local velocity direction order

Fig. 6 Performance of FOFA-based single-layer UAV swarm with 300 UAVs

forces of UAVi and other swarm members at time t can be written as

$$u_i(t) = f_i^{\text{att}}(t) + f_i^{\text{rep}}(t) + f_i^{\text{align}}(t) + f^{\text{wind}}(t), \tag{40}$$

where $f^{\text{wind}}(t)$ denotes air flow at time t. Let $c_w = 0.1$, the status of UAV swarms with different scales in a multi-directional time sequence air flow environment are shown in Fig. 8. In Fig. 8a, there are 100 UAVs, and it can be seen that after 50 iterations, all the UAVs move in the same direction. When the UAV swarm converges, the wind direction is towards the upper right corner. Figure 8b–d show UAV's positions and directions under changing air flow when the scales of UAV swarms are 200, 300 and 400, respectively. All the UAV swarms can achieve convergence under wind environment, which indicates that FOFA also has a good performance under physical constraints.

FOFA in a multilayer UAV swarm

To better perform missions, UAV swarms are often divided into several layers, and the most widely used are leader-

Table 1 Average t_c and t_s of single-layer UAV swarms based on FOFA

	Number of UAVs	Order of FOFA									
		0.1	0.2	0.3	0.4	0.5	0.6	0.7	0.8	0.9	1.0
t_c	50	13.6	14.3	13.6	13.4	14.3	13.7	13.7	13.3	13.8	**13.1**
	100	16.8	16.6	15.6	17.1	14.8	16.4	**15.5**	16.3	15.7	16.0
	200	22.2	20.2	19.8	20.9	**19.3**	20.0	20.9	21.8	21.0	22.5
	300	**37.2**	38.9	37.8	43.6	46.4	49.6	54.2	56.7	56.1	56.1
	400	60.7	**59.1**	68.8	88.0	103.9	111.8	116.8	118.3	118.7	118.3
t_s	50	22.9	22.8	22.1	21.6	21.2	21.1	20.5	20.7	20.4	**20.1**
	100	24.4	23.5	22.8	22.6	22.3	21.9	21.5	21.3	21.2	**21.1**
	200	28.3	28.7	**28.1**	28.3	28.2	28.3	29.0	29.0	28.2	29.1
	300	35.4	35.6	**34.5**	38.5	38.7	45.1	46.9	50.07	51.1	53.0
	400	46.3	**46.2**	48.6	57.6	74.6	89.1	102.1	106.6	113.1	116.0

follower swarms. Here, we use the hierarchical strategy in Ref. [10], where particles are divided into leaders and followers by their contribution weight. The parameters are set as follows: the contributions of leaders and followers are 10 and 1, respectively, and all UAVs can communicate with their neighbors. The numbers of leaders and followers are $M = 5$ and $N - M$, and the other parameters are the same as those of the single-layer UAV swarm given in Sect. 4.2.2. The results are shown in Fig. 9 and. Similar to the single-layer UAV swarms, when the number of UAVs is small, there is almost no improvement, and as the scale increases, the time to achieve convergence is greatly reduced.

The specific convergence time corresponding to the various fractional orders of FOFA is shown in Table 2, where bolded font indicates optimal convergence time. We can see that both the overall and local convergence times are greatly decreased by the FOFA with an increase in the number of UAVs, and a larger scale corresponds to better performance.

The above results lead to the conclusion that when the scale of the UAV swarm is large ($N > 300$), the FOFA greatly improves the convergence rate regardless of whether it is hierarchical or not. Interestingly, we find that in both Table 1 and Table 2, the optimal order for convergence time is generally reduced with the increase of scale of UAV swarm, and we notice that smaller fractional order indicates more consideration of historical information. Does that indicate that there exists a certain relationship between the historical information (fractional order of FOFA) and the convergence rate of UAV swarm? In the next section, this problem is analyzed in detail.

Correlation analysis between α and the performance of the UAV swarm

To detect correlations between different performance indicators, we can observe their measurements on the same UAV swarm. Different performance indicators result in different sorting sequences. Here, Kendall"s tau sequence correlation [43] is used to measure the correlation between fractional orders and the performance of the UAV swarm, which is defined as follows.

Let $X = (x_1, x_2, \ldots, x_n)$ and $Y = (y_1, y_2, \ldots, y_n)$ be two random sequences and $(x_1, y_1), (x_2, y_2), \ldots, (x_n, y_n)$ be a set of observations from X and Y, so that all the values of x_i and y_i are unique. Each pair of (x_i, y_i) and (x_j, y_j), where $i < j$, has three kinds of relationships, namely, concordant, discordant and neither concordant nor discordant. They are said to be concordant if the ranks for both elements (more precisely, the sort order by x and by y) agree: if both $x_i > x_j$ and $y_i > y_j$; or if both $x_i < x_j$ and $y_i < y_j$. They are said to be discordant if $x_i > x_j$ and $y_i < y_j$ or if $x_i < x_j$ and $y_i > y_j$. If $x_i = x_j$ and $y_i = y_j$, the pair is neither concordant nor discordant. Then, Kendall's tau coefficient is defined as

$$\tau = \frac{c - d}{n(n-1)/2}, \tag{41}$$

where c is the number of concordant pairs and d is the number of discordant pairs.

The time to achieve overall convergence t_c and local convergence t_s of the single-layer and leader-follower UAV swarm at different scales ($N = 50, 100, 200, 300, 400$) based on FOFA is shown in Tables 3 and 4, respectively.

Now, we calculate Kendall's tau coefficient between fractional order α and overall convergence time t_c as well as local convergence time t_s in single-layer and leader-follower UAV swarms. First, let $X = (\alpha_1, \alpha_2, \ldots, \alpha_{10})$ be the sequence of α, where $\alpha_1 = 0.1, \alpha_2 = 0.2, \ldots, \alpha_{10} = 1$, and $T_c = (t_{c1}, t_{c2}, \ldots, t_{c10})$ and $T_s = (t_{s1}, t_{s2}, \ldots, t_{s10})$ be the sequence of overall convergence time t_c and local convergence time t_s corresponding to α, where the elements of T_c and T_s can be seen in Tables 1 and 2. For instance, for a single-layer UAV swarm with 300 UAVs, its sequences of X, T_c and T_s are shown in Table 3, and the indicators are

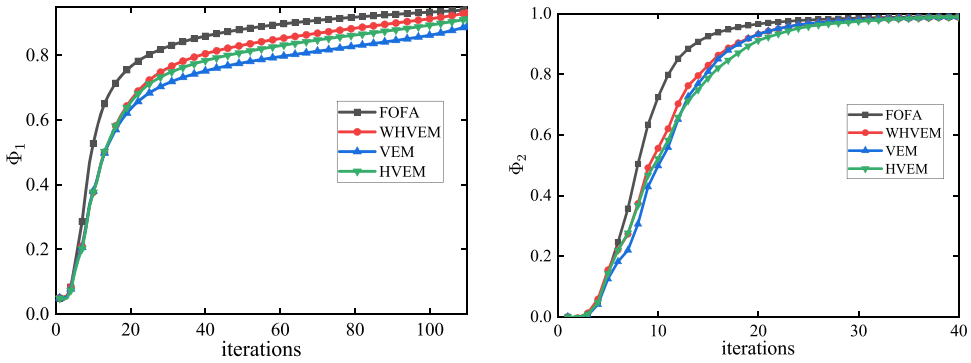

(a) Overall velocity direction order **(b)** Local velocity direction order

Fig. 7 Comparison between FOFA, WHVEM, VEM and HVEM

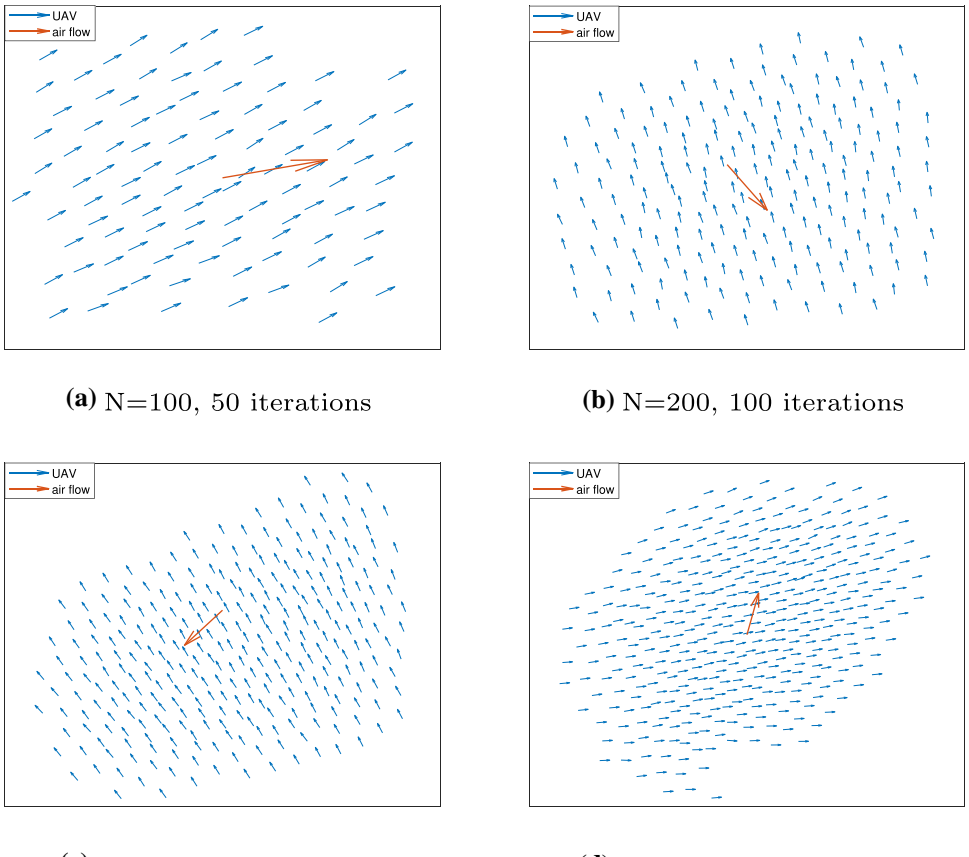

(a) N=100, 50 iterations **(b)** N=200, 100 iterations

(c) N=300, 150 iterations **(d)** N=400, 250 iterations

Fig. 8 FOFA of UAV swarms in wind environment

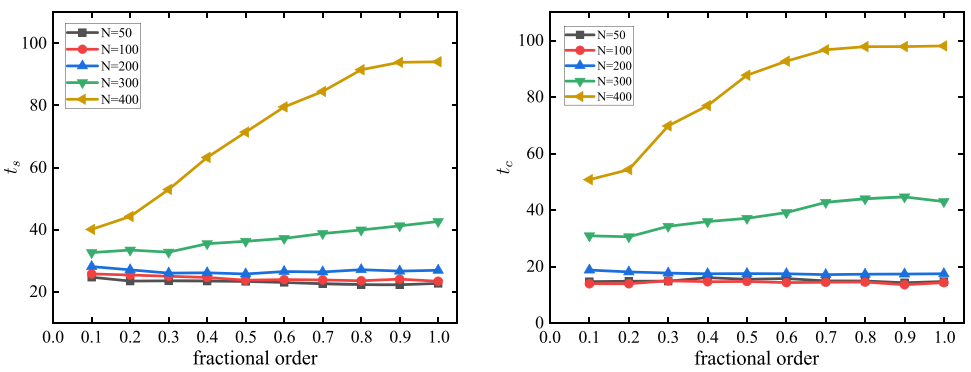

(a) Average overall convergence time **(b)** Average local convergence time

Fig. 9 Convergence time of FOFA-based leader-follower UAV swarms at different scales and fractional orders

Table 2 Average t_c and t_s of leader-follower UAV swarms based on FOFA

	Number of UAVs	Order of FOFA									
		0.1	0.2	0.3	0.4	0.5	0.6	0.7	0.8	0.9	1.0
t_c	50	14.7	14.8	14.8	16.1	15.5	15.7	14.9	14.9	**14.3**	14.7
	100	13.9	13.9	15.0	14.6	14.7	14.3	14.4	14.5	**13.5**	14.3
	200	20.1	**18.3**	20.2	22.5	20.9	22.2	23.1	23.2	23.1	24.2
	300	30.9	**30.5**	34.3	35.9	37.1	39.1	42.7	44.0	44.7	43.0
	400	**50.8**	54.3	69.8	77.0	87.7	92.7	96.7	97.8	97.8	98.1
t_s	50.0	24.7	23.5	23.5	23.4	23.3	23.0	22.6	22.4	**22.3**	22.7
	100	25.8	25.4	25.0	24.6	23.7	23.9	23.8	**23.6**	24.1	23.4
	200	28.1	27.1	26.0	26.1	**25.7**	26.5	26.4	27.1	26.7	26.9
	300	**32.6**	33.4	32.8	35.5	36.3	37.2	38.7	39.9	41.2	42.6
	400	**40.1**	44.3	52.9	63.3	71.4	79.5	84.5	91.5	93.9	94.0

Table 3 Sequence of single-layer UAV swarm with 300 UAVs

X	0.10	0.20	0.30	0.40	0.50	0.60	0.70	0.80	0.90	1.00
T_c	37.22	38.91	37.76	43.59	46.37	49.61	54.16	56.73	56.05	56.14
T_s	35.40	35.56	34.48	38.52	38.68	45.06	46.90	50.07	51.09	52.99

Table 4 Vulnerability order of single-layer UAV swarm with 300 UAVs

X	$\alpha_1 <$	$\alpha_2 <$	$\alpha_3 <$	$\alpha_4 <$	$\alpha_5 <$	$\alpha_6 <$	$\alpha_7 <$	$\alpha_8 <$	$\alpha_9 <$	α_{10}
T_c	$T_{c1} <$	$T_{c2} <$	$T_{c3} <$	$T_{c4} <$	$T_{c5} <$	$T_{c6} <$	$T_{c7} <$	$T_{c10} <$	$T_{c9} <$	T_{c8}
T_s	$T_{s3} <$	$T_{s1} <$	$T_{s2} <$	$T_{s4} <$	$T_{s5} <$	$T_{s6} <$	$T_{s7} <$	$T_{s8} <$	$T_{s9} <$	T_{s10}

Table 5 Kendall's tau sequence coefficient of UAV swarm based on FOFA

Type	Number of UAVs	Between α and T_c	Between α and T_s
Single-layer	50	0	0
	100	0	0
	200	0.33	0.38
	300	0.87	0.91
	400	0.91	0.96
Leader-follower	50	0	0
	100	0	0
	200	0	0.1
	300	0.87	0.96
	400	1	1

ranked in Table 4. Then, we calculate Kendall's tau sequence correlation between these sequences. The sequence correlation coefficient results of the fractional order and overall convergence time are 0.87 and that with local convergence time is 0.91. Therefore, when the scale is 300, the correlation between the historical information and the performance of the UAV swarm is strong. Similar to the above method, all the sequence correlation coefficient results are shown in Table 5.

From Table 5, we can see that when the scale of the UAV swarm is less than 300, the coefficient value is very small; thus, it appears that there is no correlation between the fractional order and performance of the UAV swarm. However, when the scale reaches $N \geq 300$, the coefficient value is close to 1, which indicates that there exists a strong correlation between the fractional order of FOFA and the convergence rate of both single-layer and multilayer UAV swarms with large scales. It should be noted that a smaller fractional order of FOFA corresponds to more consideration of historical information in the updating process. Therefore, we conclude that historical information significantly influences the convergence rate of large-scale UAV swarms; moreover, the more historical information is taken into consideration, the faster convergence is obtained.

Conclusion

The fractional-order flocking algorithm (FOFA) of UAV swarms is proposed in this paper, which greatly improves the convergence rate of UAV swarms, especially for large-scale UAV swarms. The main feature of the proposed FOFA is that historical information is considered in the updating process of the UAV swarm by the inherent "memory" property of fractional calculus. Then we analyzed the convergence of the FOFA in theory. By exploiting graph theory, a sufficient convergence condition is given. To verify the effectiveness of FOFA in reducing convergence time of UAV swarms, simulations are carried out at different swarm scales and types. Furthermore, we find that the correlation between the fractional order of the FOFA and the convergence rate of the large-scale UAV swarm is quite strong; in other words, the more historical information is considered in the updating process, the faster the convergence rate of the large-scale UAV swarm. Thus, the fractional order can be used as an important parameter to control the convergence rate of the large-scale UAV swarm. In future work, more practical situations for UAV swarms, such as navigation and obstacle avoidance, can be studied based on this paper.

Acknowledgements This work was supported by National Natural Science Foundation of China, No. 62273356; National Talent Project of China, No. 2022-JCJQ-ZQ-001; Provincial Primary Research & Development Plan of Jiangsu, China, No. BE2021729 High-level Talents Innovation Project, China, No. KYZYJQJY2101.

Declarations

Conflict of interest The authors declare that they have no known competing financial interests or personal relationships that could have appeared to influence the work reported in this paper.

References

1. Ling H, Mclvor GE, Westley J, van der Vaart K, Vaughan RT, Thornton A, et al. (2019) Behavioural plasticity and the transition to order in jackdaw flocks. Nat Commun 10. https://doi.org/10.1038/s41467-019-13281-4
2. Berlinger F, Gauci M, Nagpal R. (2021) Implicit coordination for 3D underwater collective behaviors in a fish-inspired robot swarm. Sci Robot 6(50). https://doi.org/10.1126/scirobotics.abd8668
3. Mayor R, Etienne-Manneville S (2016) The front and rear of collective cell migration. Nat Rev Mol Cell Biol 17(2):97–109. https://doi.org/10.1038/nrm.2015.14
4. Ling H, McIvor GE, van der Vaart K, Vaughan RT, Thornton A, Ouellette NT (2019) Costs and benefits of social relationships in the collective motion of bird flocks. Nat Ecol Evolut 3(6):943–948. https://doi.org/10.1038/s41559-019-0891-5
5. Yan C, Xiang X, Wang C, Li F, Wang X, Xu X, et al (2023) PASCAL: population-specific curriculum-based MADRL for collision-free flocking with large-scale fixed-wing UAV swarms. Aerosp Sci Technol 133. https://doi.org/10.1016/j.ast.2022.108091
6. Wang W, Wang L, Wu J, Tao X, Wu H (2022) Oracle-Guided deep reinforcement learning for large-scale multi-UAVs flocking and navigation. IEEE Trans Veh Technol 71(10):10280–10292. https://doi.org/10.1109/TVT.2022.3184043
7. Jia Y, Du J, Zhang W, Wang L (2017) Three-dimensional leaderless flocking control of large-scale small unmanned aerial vehicles. IFAC Papersonline 50(1):6208–6213. https://doi.org/10.1016/j.ifacol.2017.08.1016
8. Liu J, He M, Xu P, Deng X (2022) Pairwise control in swarm flocking with application to UAVs. Eng Appl Artif Intell 114. https://doi.org/10.1016/j.engappai.2022.105023
9. Olfati-Saber R (2006) Flocking for multi-agent dynamic systems: algorithms and theory. IEEE Trans Automat Control 51(3):401–420. https://doi.org/10.1109/TAC.2005.864190
10. Jia Y, Vicsek T (2019) Modelling hierarchical flocking. New J Phys 24:21. https://doi.org/10.1088/1367-2630/ab428e
11. Vicsek T, Czirok A, Benjacob E, Cohen I, Shochet O (1995) Novel type of phase-transition in a system of self-driven particles. Phys Rev Lett 75(6):1226–1229. https://doi.org/10.1103/PhysRevLett.75.1226
12. Liu X, Xiang X, Chang Y, Yan C, Zhou H, Tang D (2021) Hierarchical weighting vicsek model for flocking navigation of drones. Drones 5(3). https://doi.org/10.3390/drones5030074
13. Liu X, Yan C, Zhou H, Chang Y, Xiang X, Tang D (2021) Towards flocking navigation and obstacle avoidance for multi-UAV systems through hierarchical weighting vicsek model. Aerospace 8(10). https://doi.org/10.3390/aerospace8100286
14. Zhao M, Su H, Wang M, Wang L, Chen MZQ (2016) A weighted adaptive-velocity self-organizing model and its high-speed performance. Neurocomputing 216:402–408. https://doi.org/10.1016/j.neucom.2016.08.008
15. Lu X, Zhang C, Huang C, Qin B . (2022) Research on swarm consistent performance of improved Vicsek model with neighbors' degree. Physica A Stat Mech Appl 15:588. https://doi.org/10.1016/j.physa.2021.126567
16. Zhao Q, Li S, Wang G, Wang C, Xie GA (2020) Local consistency algorithm to shorten the convergence time and improve the robustness of self-propelled swarms. Chin Autom Cong 2020:4153–4157
17. Couzin I, Krause J, James R, Ruxton G, Franks N (2002) Collective memory and spatial sorting in animal groups. Journal Theor Biol. 218(1):1–11. https://doi.org/10.1006/jtbi.2002.3065
18. Zhang X, Jian M, Jia S, Li X (2017) Optimal fractional order of self-propelled particles in the synchronization motion. In: Proceedings of the 36th chinese control conference. Chinese Control Conference, 11374–11378
19. Su H, Ye Y, Chen X, He H (2021) Necessary and sufficient conditions for consensus in fractional-order multiagent systems via sampled data over directed graph. IEEE Trans Syst Man Cybern Syst 51(4):2501–2511. https://doi.org/10.1109/TSMC.2019.2915653
20. Zhang Y, Wu H, Cao J (2022) Group consensus in finite time for fractional multiagent systems with discontinuous inherent dynam-

ics subject to Holder growth. IEEE Trans Cybern 52(6):4161–4172. https://doi.org/10.1109/TCYB.2020.3023704
21. Yao K, Chen H, Peng WL, Wang Z, Yao J, Wu Y (2021) A new method on Box dimension of Weyl-Marchaud fractional derivative of Weierstrass function. Chaos Solit Fract. https://doi.org/10.1016/j.chaos.2020.110317
22. Liang YS (2018) Fractal dimension of Riemann-Liouville fractional integral of 1-dimensional continuous functions. Fract Calc Appl Anal 21(6):1651–1658. https://doi.org/10.1515/fca-2018-0087
23. Pandey V, Holm S (2016) Connecting the grain-shearing mechanism of wave propagation in marine sediments to fractional order wave equations. J Acoust Soc Am 140(6):4225–4236. https://doi.org/10.1121/1.4971289
24. Chen W, Hu S, Cai W (2016) A causal fractional derivative model for acoustic wave propagation in lossy media. Arch Appl Mech 86(3):529–539. https://doi.org/10.1007/s00419-015-1043-2
25. Pires EJS, Machado JAT, Oliveira PBdM, Cunha JB, Mendes L (2010) Particle swarm optimization with fractional-order velocity. Nonlinear Dyn 61(1–2):295–301. https://doi.org/10.1007/s11071-009-9649-y
26. Cui Y, Hu W, Rahmani A (2023) Fractional-order artificial bee colony algorithm with application in robot path planning. Eur J Oper Res 306(1):47–64. https://doi.org/10.1016/j.ejor.2022.11.007
27. Yousri D, AbdelAty AM, Al-qaness MAA, Ewees AA, Radwan AG, Abd Elaziz M (2022) Discrete fractional-order Caputo method to overcome trapping in local optima: Manta Ray Foraging Optimizer as a case study. Expert Syst Appl 15:192. https://doi.org/10.1016/j.eswa.2021.116355
28. Dong Y, Liao W, Wu M, Hu W, Chen Z, Hou D (2022) Convergence analysis of Riemann–Liouville fractional neural network. Math Methods Appl Sci 45(10):6378–6390. https://doi.org/10.1002/mma.8175
29. Sun H, Zhang Y, Baleanu D, Chen W, Chen Y (2018) A new collection of real world applications of fractional calculus in science and engineering. Commun Nonlinear Sci Numer Simul 64:213–231. https://doi.org/10.1016/j.cnsns.2018.04.019
30. Boudaoui A, Moussa YEH, Hammouch Z, Ullah S (2021) A fractional-order model describing the dynamics of the novel coronavirus (COVID-19) with nonsingular kernel. Chaos Solitons Fract. https://doi.org/10.1016/j.chaos.2021.110859
31. Kepten E, Bronshtein I, Garini Y (2011) Ergodicity convergence test suggests telomere motion obeys fractional dynamics. Phys Rev 83(4,1). https://doi.org/10.1103/PhysRevE.83.041919
32. Sales Teodoro G, Tenreiro Machado JA, Capelas de Oliveira E (2019) A review of definitions of fractional derivatives and other operators. J Comput Phys 1(388):195–208. https://doi.org/10.1016/j.jcp.2019.03.008
33. Grzymkowski L, Trofimowicz D, Stefanski TP (2020) Stability analysis of interconnected discrete-time fractional-order LTI state-space systems. Int J Appl Math Comput Sci 30(4), 649–658. https://doi.org/10.34768/amcs-2020-0048
34. Stanislawski R, Latawiec KJ (2013) Stability analysis for discrete-time fractional-order LTI state-space systems. Part II: New stability criterion for FD-based systems. Bull Polish Acad Sci Tech Sci. 61(2):363–370. https://doi.org/10.2478/bpasts-2013-0035
35. Shahamatkhah E, Tabatabaei M (2020) Leader-following group consensus of discrete-time fractional-order double-integrator multi-agent systems. ISA Trans 106:262–270. https://doi.org/10.1016/j.isatra.2020.07.015
36. Mesbahi M, Egerstedt M (2010) Graph theoretic methods in multiagent networks. In: Graph Theoretic Methods in Multiagent Networks. Princeton University Press
37. Fei C, Wei R (2021) Multi-agent control: a graph-theoretic perspective. J Syst Sci Complex 34(5):1973–2002. https://doi.org/10.1007/s11424-021-1218-6
38. Fu X, Pan J, Wang H, Gao X (2020) A formation maintenance and reconstruction method of UAV swarm based on distributed control. Aerosp Sci Technol 104. https://doi.org/10.1016/j.ast.2020.105981
39. Zohdi TI (2018) Multiple UAVs for mapping: a review of basic modeling, simulation, and applications. In: Gadgil A, Tomich T, editors. Annual review of environment and resources, vol 43. 43 of Annual Review of Environment and Resources, p. 523–543
40. Wu J, Yu Y, Ma J, Wu J, Han G, Shi J et al (2021) Autonomous cooperative flocking for heterogeneous unmanned aerial vehicle group. IEEE Trans Veh Technol 70(12):12477–12490. https://doi.org/10.1109/TVT.2021.3124898
41. Shahamatkhah E, Tabatabaei M (2018) Leader-following consensus of discrete-time fractional-order multi-agent systems. Chin Phys B 27(1). https://doi.org/10.1088/1674-1056/27/1/010701
42. Cavagna A, Giardina I (2014) Bird flocks as condensed matter. Annu Rev Condens Matter Phys 5(1):183–207. https://doi.org/10.1146/annurev-conmatphys-031113-133834
43. Brophy AL (1986) An algorithm and program for calculation of Kendall's rank correlation coefficient. Behav Res Methods Instrum Comput 18(1):45–46